Environmental Science

AIMS Environmental Science, 12(6): 999–1030.
DOI: 10.3934/environsci.2025044
Received: 31 August 2025
Revised: 29 November 2025
Accepted: 11 December 2025
Published: 17 December 2025

http://www.aimspress.com/journal/environmental

Research article

Study of PVA fibers to improve the corrosion resistance of Suzhou Typical River Mucky Clay

Yuexiang Wang[1,*], Haigao Jia[1] and Kaiyu Chen[2]

[1] Suzhou University of Science and Technology, Suzhou, Jiangsu, China
[2] CSCEC International Construction Co., Ltd., Suzhou, Jiangsu, China

* **Correspondence:** Email: wyxcjy@sina.cn.

Abstract: To investigate the effect of Polyvinyl Alcohol (PVA) fiber incorporation on the erosion resistance of soil under different environmental conditions, this study selected fiber length and fiber content as variables and systematically compared the performance difference between fiber-reinforced soil and plain soil through dry and wet cycles, freeze-thaw cycles, sulfate erosion, and scouring tests. The fiber soil was found to have significant erosion resistance compared to the plain soil. The results showed that, for dry-wet cycling, the addition of PVA fibers effectively enhances the soil sample's resistance. Particularly, when the fiber content ranges from 0.5% to 0.8%, the soil sample's resistance to dry-wet cycles is significantly improved. Moreover, the influence of fiber content on enhancing the dry-wet cycling performance of the sample is more pronounced than that of fiber length. Shrinkage tests showed that the soil undergoes three distinct stages during the drying process: constant rate, deceleration, and residual phases. Under the action of freeze-thaw cycles, specimens containing PVA fibers demonstrate good deformation resistance and high unconfined compressive strength and do not appear to be damaged in the process of freezing and thawing, indicating good freeze-thaw resistance. Meanwhile, the effect of fiber length on the strength-loss rate is minor, suggesting that the freeze-thaw resistance of the specimens is relatively insensitive to fiber length. For the sulfate erosion resistance test, with an increase in fiber content, the strength of the specimen improves, and its strength loss rate is significantly reduced, whereas the influence of fiber length on the specimen remains limited. In the scouring test, soil samples show good scour resistance after fiber content, and the scour growth rate decreases with time.

Keywords: PVA fiber; corrosion resistance; fiber content; fiber length; unconfined compressive strength; damage pattern

1. Introduction

Soft soil is widely distributed in coastal plains, deltas, and areas surrounding lakes in China. Due to its characteristics of high-water content, low strength, high compressibility, and large pore ratio [1], significant settlement and deformation, low strength, and other problems often occur in road engineering, coastal engineering, and various types of infrastructure projects. These issues make it difficult for soft soil to meet the requirements for bearing capacity and deformation control in engineering applications [2–3].

To improve the engineering performance of soft ground, it is usually reinforced with a mixture of cement, quicklime, crushed stone, and fly ash. However, although conventional reinforcement methods can improve the engineering performance of soft ground to a certain extent, they have a limited effect on improving the cracking and tensile strength of the soil, and the performance of eroded soil is significantly reduced in harsh environments [4], which will directly affect its durability. Therefore, it is of great significance to explore more effective improvement measures to enhance the erosion resistance of soft soils in different environments.

In recent years, polypropylene fibers, basalt fibers, and steel fibers have been widely used as reinforcing materials and have made significant progress in the field of cementitious composites. However, these fibrous materials generally suffer from poor dispersion and high production costs, which limit their further application in engineering fields [5]. PVA fiber made from polyvinyl alcohol is a synthetic fiber with high strength, high modulus, and good hydrophilicity that can be dissolved in water for soil curing. As a highly stable, alkali-resistant, environmentally friendly, and biodegradable material, it has a strong interfacial bonding capacity and provides a new method for soft soil improvement [6].

Research on the application of PVA fibers in soils by scholars from various countries has laid the foundation for its development, leading to the expansion of its application [7–13]. For example, Zhang P, Li Q, Wang J, et al. [14] found that the incorporation of PVA fibers significantly enhanced the durability of cementitious composites based on cracking ratio and freeze-thaw cycle tests. When the fiber content was lower than 1.2%, the cracking durability index of the material increased with the increase of fiber content. However, when the content increased from 0.9% to 1.2%, a decreasing trend in the freeze-thaw durability index was observed. Lei B, Pang S, Sun J, et al. [15] systematically investigated the evolution of freeze-thaw durability in fiber-reinforced stabilized soil (FSS) formed by incorporating polypropylene fibers. The study revealed that after freeze-thaw cycles, the peak strength, deformation modulus, and cohesion of all specimens gradually declined. Under identical freeze-thaw conditions, the fiber-reinforced specimens consistently demonstrated superior performance compared with the unreinforced specimens. Zeng Y, Peng L, Ma B, et al. [16] evaluated nano-silica-modified lightweight cementitious materials with varying multi-walled carbon nanotubes (MWCNT) contents under combined freeze-thaw cycling and chloride exposure. Their results showed that MWCNTs enhanced matrix densification, improved compressive strength, and reduced chloride ingress, with 0.1

wt% providing the most effective improvement. The study demonstrated that an appropriate MWCNT dosage can significantly enhance the durability of lightweight cement-based composites in such coupled environments. Zeng Y, Li X, Tang A, et al. [17] examined the axial compression performance of lightweight aggregate concrete reinforced with basalt and polyacrylonitrile fibers under freeze-thaw deterioration. Their findings showed that while fiber addition slightly increased the peak compressive stress, it did not substantially alleviate the brittleness induced by cyclic damage, as progressive freeze-thawing still promoted microcrack growth and a significant decline in elastic modulus. Optimal dosages of about 0.5% Basalt Fiber (BF) and 1.0% Polyacrylonitrile Fiber (PANF) reduced axial strength loss after 300 cycles from 47.9% to 24.5% and 29.1%, respectively. The study also introduced predictive models for peak stress and modulus, together with an energy-based toughness assessment, offering useful references for designing durable fiber-reinforced Lightweight aggregate concrete (LWAC) in cold environments. Qu W, Maimt N, Qu J [18] investigated the modification of cement-bound soil using zeolite and palm fiber. The study demonstrated that composite materials with optimized proportions significantly enhance durability under salt erosion, wet-dry cycling, and freeze-thaw cycling. Compared with ordinary cement-bound soil, the composite exhibited minimal strength and mass loss after testing. Microscopic analysis revealed the mechanism behind the performance enhancement. Dhakal S, Kolay P, Puri V [19] investigated the reinforcement of highly compressible clay using Calcium Sulfo-Aluminate Cement (CSAC) and polypropylene fibers. The results showed that specimens prepared with 10.0% CSAC and 1.0% fiber fully resisted standard dry-wet cycling damage. Specimens containing 0.5% and 1.0% fibers both passed all freeze-thaw cycles. After the durability tests, the surviving specimens retained significant unconfined compressive strength. Youn I, Bang S, Jeong Y, et al. [20] examined the durability of earth bricks stabilized with lime and natural short-fiber composites. Dry-wet cycling caused a 63% reduction in strength and a 45% decrease in relative dynamic modulus. Nevertheless, the eco-stabilizer markedly increased the shear strength of the soil matrix, thereby improving the overall durability of the earth bricks. Liang Z, Yan C, Cao Y, et al. [21] evaluated bio-polymer-fiber composite modified loess (BFCL), where a composite ratio of 0.5% fiber and 1.0% bio-polymer maximized shear strength. After eight freeze-thaw cycles, the material properties stabilized, with its outstanding erosion resistance attributed to the synergistic effect of fiber confinement and bio-polymer cementation. Wan L, Zhao Y, Yu M, et al. [22] found that the durability and fracture toughness of the specimen series showed a tendency to increase and then decrease with increasing PVA content under different numbers of salt water freeze-thaw cycles. Also, PVA fiber-reinforced cementitious composites (PFRCC) exhibited the best durability performance at a fiber content of 0.5%. Zhang P, Sun X, Wei J, et al. [23] explored the effect of polyvinyl alcohol (PVA) fiber content on the durability of cementitious composites in a humidity-heat-salt coupling environment through a series of durability tests. The results showed that the addition of 1.2% PVA fiber content provided the most ideal durability enhancement, and fiber addition was beneficial. Yan Chang Wang et al. [24] investigated the mechanical properties of fiber concrete by controlling the content and length of PVA fibers during chloride salt erosion and sulfate erosion tests. The experimental results showed that when the fiber length was 12 mm and the fiber content was 1.2 kg/m^3, the specimen had the best effect on the salt erosion resistance. Ma Nan et al. [25] found that the compressive strength, dynamic modulus of elasticity, and tensile strength of PVA fiber concrete first increased and then decreased after 15 cycles of dry-wet cycling in 5% sulfate solution, and the specimen with a fiber volume content of

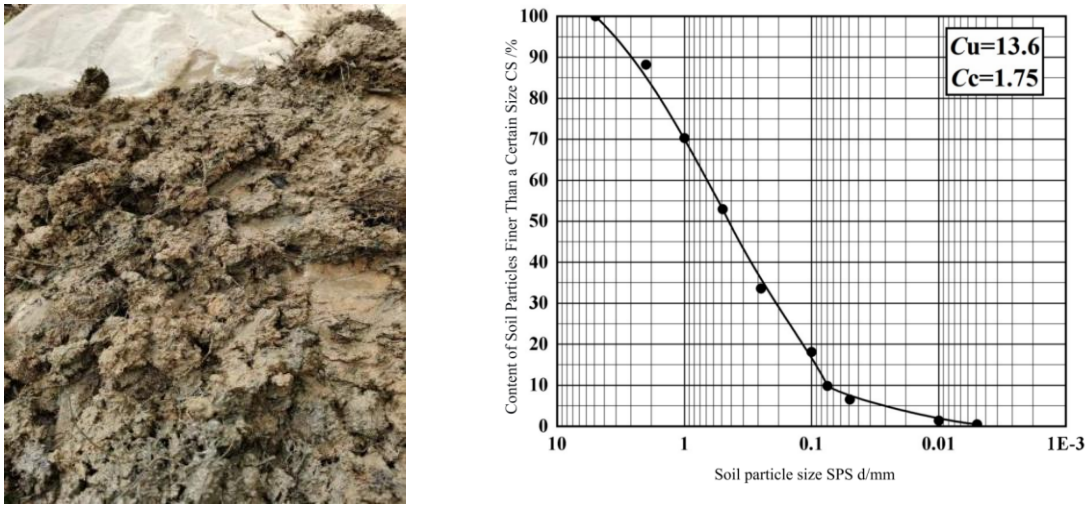
2.0 kg/m³ demonstrated the best resistance to sulfate stress. Zhao Xiaoming et al. [26] investigated the durability of PVA fiber concrete under freeze-thaw cycles by varying the PVA fiber admixture from 0.05% to 0.15% and fiber length from 8 to 12 mm. The tests showed that specimens with an 8 mm fiber length and 0.10% fiber content exhibited the best freeze-thaw resistance, with a 40% reduction in mass loss rate. Tan H, Ma C, Li S, et al. [27] conducted laboratory tests to evaluate the effects of fiber type, contents, and lengths on the performance of underwater flowable solidified soil (UFSS). The results showed a threshold effect for fiber enhancement of unconfined compressive strength (UCS) and scour resistance: both properties initially increased with rising fiber content or length, then declined as excess fibers produced adverse effects. The optimal performance was achieved with PVA fibers at 0.3% content and 6 mm length, while basalt and glass fibers performed best at 0.2% content and 6 mm length. Li L, Li S, Li W, et al. [28] utilized industrial waste rice husk ash and polypropylene fibers to prepare reinforced soil. Optimal strength was achieved at 5% rice husk ash, 0.7% polypropylene fiber, and 0.6 mol/L NaOH. Rainfall erosion model tests confirmed that the erosion volume of fiber-reinforced soil slopes was significantly lower than that of unmodified soil slopes, indicating that fiber incorporation effectively improves slope resistance to erosion and sliding.

In this paper, in view of the limitations of traditional reinforcement materials in soft soil reinforcement projects, combined with the characteristics of the fiber material itself, as well as the production cost of fibers, an appropriate amount of PVA fiber was selected and added to cement and quicklime soil specimens. Through a series of corrosion tests, such as wet-dry cycles, freeze-thaw cycles, anti-sulfate erosion tests, and scouring tests, the effects of fiber incorporation and fiber length on the corrosion resistance of fiber-reinforced soil were analyzed. The influence of fiber content and length on the erosion resistance of fibrous soil was discussed in detail.

2. Test materials and methods

2.1. Selection of soil samples

The soil samples used in this experiment, consisting of silty soil, were obtained from a river channel in Suzhou City, Jiangsu Province, China. Because the raw soil contains leaves, twigs, plastics, and other debris, it was air-dried in a cool, ventilated place, crushed with a rubber hammer, filtered through a 2 mm sieve to remove other debris, placed in a drying box at a constant temperature for 4 h, and then kept as a sample for subsequent experiments. According to the Standard for Geotechnical Test Methods (GB/T50123-2019) [29], the physical properties were tested, and the results are shown in Table 1. The raw soil exhibits a light grayish-yellow appearance, is saturated, possesses a high natural moisture content, and demonstrates high compressibility. Its appearance and gradation are shown in Figure 1. Based on the plasticity index (Ip) and liquid limit (IL) values in Table 1, the undisturbed soil is determined to be in a plastic state.



Raw Soil **Soil particle size distribution curve**

Figure 1. Raw soil and its particle size distribution chart.

Table 1. Physical indicators of the soil.

ρ(g/cm^3)	W %	W_p %	W_L %	Ip	I_L	e	G_S
1.77	60.94%	28.9	45.7	16.8	1.9	1.43	2.63

2.2. Selection of solidification materials and PVA fibers

P.O42.5 cement has become an indispensable building material in civil engineering due to its excellent plastic deformation properties before initial setting and outstanding compressive strength and durability after hardening. The addition of calcium chloride, a quick-setting agent, can significantly shorten the setting time of cement, enhance early strength, and improve the compatibility of the mixture. Therefore, P.O42.5 cement was chosen as the primary curing agent, and calcium chloride was used as the auxiliary curing agent. The materials are shown in Figure 2, and the specific parameters are detailed in Tables 2 and 3.

Table 2. P.O42.5 cement performance parameters.

Incipient condensation time (min)	Time of final coagulation (min)	7 d unconfined compressive strength (MPa)	28 d unconfined compressive strength (MPa)	7 d tensile strength (MPa)	28 d tensile strength (MPa)	Specific surface (m^2•kg^{-1})	ρ (g/cm^{-3})	Heat loss %
175	235	27.5	49	5	19	361	3.05	4

Table 3. Calcium chloride: elements and properties.

ρ (g/cm^3)	pH	Ca (%)	CI (%)	O (%)	H (%)	Clarity test
2.15	9	27.26	48.23	21.77	2.74	4

PVA fiber is a white synthetic fiber made from polyvinyl alcohol through a spinning process. Its excellent high strength, strong deformation resistance, long-term durability, and outstanding alkali and weather resistance ensure stable performance during service. That, together with it being non-toxic and non-polluting, justified its selection as a reinforcing material. The main performance parameters are shown in Table 4.

Table 4. Physical and performance parameters of PVA fibers.

ρ (g/cm^3)	Caliber (μm)	Average length (mm)	Tensile strength (MPa)	Modulus of elasticity (MPa)	Alkali resistance (MPa)	Dispersibility (rank)
1.25–1.35	10–20	10–50	1000–1500	30–50	Favorable	1–3

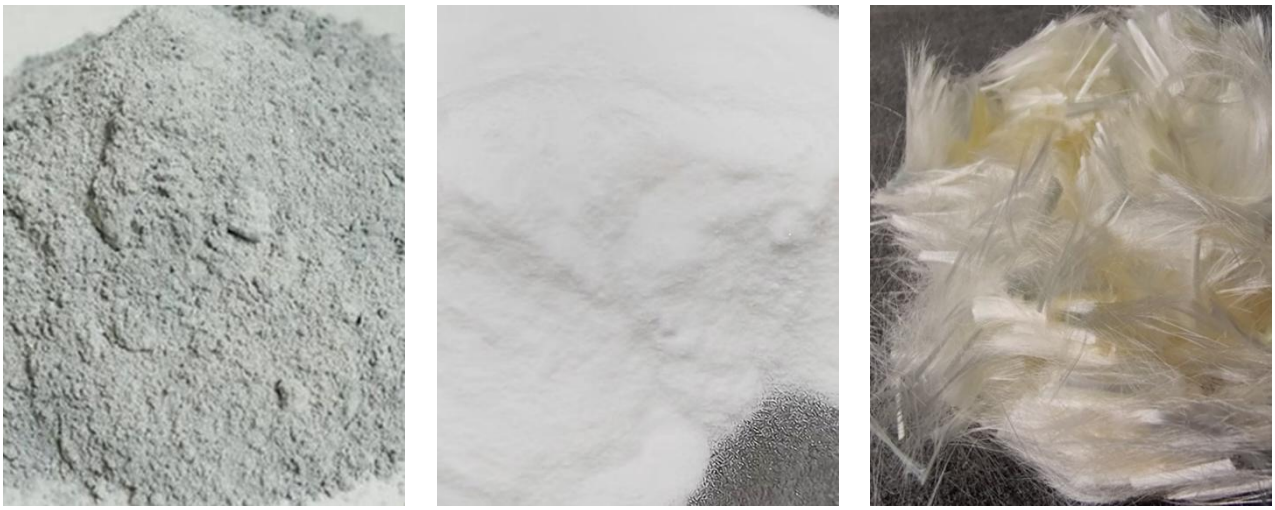


Figure 2. Cement, calcium chloride, and PVA fiber.

2.3. Sample preparation

The raw material content in the test was based on the mass of dry soil. A remolded silt soil with a water content of 60% was used, and the proportioning design took into account the factors affecting the physical and mechanical properties of the soil. PVA fiber content below 0.1% showed limited improvement in cohesion, while fiber content above 0.4% resulted in a significant decrease in post-peak cohesion [30]. Therefore, four fiber contents of 0.1%, 0.3%, 0.5%, and 0.8% were selected in this study. Fiber lengths of 3, 6, and 9 mm were used. Parameter ranges were designed with reference to previous literature [31–32], and cement and calcium chloride contents of 10% and 2% were selected.

To reduce testing errors, three parallel specimens were prepared for each mixing ratio. Based on

the calculated material proportions, each component was accurately weighed. Calcium chloride was dissolved in water and mixed thoroughly, while the fibers were added to ensure uniform dispersion. The cement was then mixed with the dry soil, after which the calcium chloride–fiber solution was slowly added and stirred evenly to obtain a homogeneous mixture. The inner wall of the mold was pre-coated with petroleum jelly to facilitate demolding, and a layered filling method was adopted, with each layer being approximately 2–3 cm thick. The specimen was compacted using a wooden hammer, the surface was leveled after the mold was filled, and it was then covered and sealed with cling film. According to the Standard for Geotechnical Test Methods [29], the specimens were demolded after being placed in a constant temperature and humidity environment for 3 days and continued to be cured until a predetermined age.

2.4. Test content and plan

2.4.1. Experimental content

To investigate the change of peak compressive strength, wet-dry cycles, freeze-thaw cycles, and salt erosion resistance tests were conducted using a YSH-2 unconfined compression (UC) tester.

Dry-wet cycle test: First, specimens were cured in a standard curing room (temperature 20 ± 2 °C, humidity ≥ 95%) for 28 days. Then, the following treatments were carried out sequentially: the specimens were dried in an oven at 70 ℃ for 12 h, and then immersed in water at 20 ± 5 °C for 12h, with the water level maintained 30 mm above the top surface of the specimen. The drying and immersing treatments were defined as a wet and dry cycle. Immediately after the cycle, an unconfined compressive strength test was carried out to assess the change in performance [33].

Freeze-thaw cycle test: after standard curing (20 ± 2 °C, humidity ≥ 95%, 28 days), the specimens were transferred to a -20 ± 2 °C environment for freezing for 12 h, and then transferred to a 20 ± 2 °C environment for thawing for 12 h. This alternating freeze-thaw process was defined as one cycle. After each cycle, an unconfined compressive strength test was executed according to the literature [34] to assess the degree of specimen performance deterioration.

Salt erosion resistance test: The specimens were cured in a standard curing room (temperature 20 ± 2 °C, humidity > 95%) for 28 days and then immersed in a 5% sodium sulfate solution with the liquid level 30 mm from the top of the specimen. The specimens were subjected to 0 (no immersion), 2, 4, and 6 cyclic tests. After the specified number of cyclic tests, the peak unconfined compressive strength of the specimens was determined, and the data were recorded. The test strictly followed the procedures specified in the literature [26].

Scour resistance test: In the unconfined compressive strength test of the control group, the specimen group with 0.3% fiber content and 3 mm fiber length demonstrated the best performance. Therefore, this group was selected as the subject for scouring tests to evaluate the scour resistance of PVA-reinforced clay under optimal modification conditions. Erosion tests are time-consuming and operationally complex. Testing only the optimal specimen group reduces experimental costs and time investment while still yielding representative erosion resistance evaluation results. Scour resistance test was performed according to the following procedure: First, the prepared soil samples were filled in a polycarbonate transparent box with dimensions of 300 mm × 200 mm × 70 mm (length × width × height), and the height of the soil samples was set to be 5 cm. The soil box was placed on a sloping

shelf at a 30° gradient, and the soil surface was flushed using an indoor artificial rainfall simulator at a rainfall intensity of 120 mm/h for 12 h. Sediment samples from the scouring were collected every 2 h according to a preset plan and subsequently weighed and measured. The tests were carried out in accordance with the relevant reference [36].

Shrinkage test: To assess the shrinkage performance, specimens of PVA fiber with 2% calcium chloride content, 10% cement content, and 3 mm length with 0.3% content were prepared. After curing for 7 days, these specimens were tested for shrinkage. The test operation was carried out in strict compliance with the provisions of the national Standard for Geotechnical Test Methods (GB/T 50123-2019) [29].

2.4.2. Experimental plan

The corrosion resistance test plan of this study contains a dry-wet cycle test, a freeze-thaw cycle test, and a salt erosion resistance test. The specific plan of the tests is detailed in Table 5.

Table 5. Corrosion resistance test plan.

Number	Fiber content (FC) (%)	Fiber length (FL) (mm)	Age (T) (days)	Number of cycles (N)
0	0	6	28	2
1	0.1			
2	0.3			
3	0.5			
4	0.8			
5	0.3	3	28	2
6		6		
7		9		
8	0.3	3	28	0
9				2
10				4
11				6

3. Results and analysis

3.1. Wet and dry cycles

3.1.1. Stress-strain curves and deformation modulus

(1) Stress-strain curves

Figure 3 demonstrates the stress-strain curves of specimens of different variables under wet and dry cycling conditions, and the corresponding detailed test data are recorded in Table 6.

Table 6. Dry and wet cycle content failure strain (ε_f).

Fiber length (FL) (mm)	Fiber content (FC) (%)	Number of cycles (N)	Failure strain (ε_f)			
			Pre-cycle	Post-cycle	Absolute value	Rate of change (%)
3	0.3	2	3.86	3.63	-0.23	-5.96
6			3.92	3.81	-0.11	-2.80
9			4.16	3.51	-0.65	-15.63
6	0.1	2	3.63	3.23	-0.40	-11.02
	0.3		3.87	3.31	-0.56	-14.47
	0.5		4.38	3.76	-0.62	-14.16
	0.8		4.52	3.83	-0.69	-15.27
3	0.3	2	3.94	3.82	-0.12	-3.05
		4	4.02	3.72	-0.30	-7.46
		6	4.25	3.13	-1.12	-26.35

According to the data in Table 6, the failure strain of the fiber-doped specimens showed a decreasing trend compared to the control group. Specifically, the percentage reduction in the failure strain was 11.02%, 14.47%, 14.16%, and 15.27% for fiber contents of 0.1%, 0.3%, 0.5%, and 0.8%, respectively. The overall percentage reduction in the failure strain increased slightly with the increase in fiber content. There was a significant difference in the percentage reduction in the breaking strength of the specimens with different fiber lengths. Specifically, the reduction rates were 5.96%, corresponding to fiber length of 3 mm, 2.80%, corresponding to fiber length of 6 mm, and 15.63%, corresponding to fiber length of 9 mm; the lowest reduction in compressive strength was observed for 6 mm fiber specimens, and the highest reduction in compressive strength was observed for 9 mm fiber specimens. Moreover, for the number of cycles, the strain at break was reduced by 3.05%, 7.46%, and 26.35%, for 2, 4, and 6 cycles, respectively. Under alternating wet and dry conditions, the failure strain of the specimens also decreased significantly with the increase in the number of cycles. This indicates that the effect of the number of cycles on the failure strain is particularly significant.

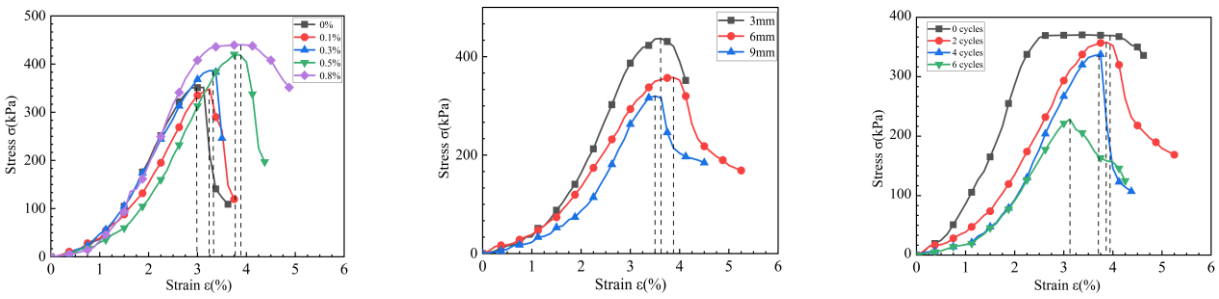


Figure 3. Stress-strain curves under different cycle conditions.

The results in Figure 3 show that the soil exhibits significant strain softening behavior during loading. Regarding fiber content, the specimen's failure strain increases with higher fiber content,

reaching its maximum at 0.8%. Furthermore, specimens with fiber content between 0.5% and 0.8% exhibited favorable ductile deformation and failure strain. This may be because higher fiber content forms a more continuous spatial network within the soil matrix, enabling broader participation in stress transfer and redistribution, thereby effectively mitigating localized stress concentration. During loading, a high fiber content continuously bridges and anchors crack propagation, significantly delaying crack penetration. Simultaneously, the abundant fibers sustain energy dissipation through pulling, sliding, and fracturing, enabling the specimens to maintain substantial deformation capacity beyond peak stress and exhibit more pronounced ductile response. Furthermore, high fiber content more effectively suppresses soil expansion, localized shear slippage, and structural loosening, enabling the material to withstand greater cumulative deformation before failure. Consequently, fiber-reinforced soil exhibits significantly enhanced failure ductility under high fiber content conditions, with failure strain markedly higher than that of low-fiber specimens.

In terms of fiber length, the specimen's failure strain increased continuously with increasing fiber length. This is due to the higher continuity of the three-dimensional spatial entanglement network formed by the fibers in the matrix as the fiber length increases [37]. This networked structure not only significantly increases the effective frictional contact area between the fibers and the soil particles but also synchronously enhances the anchoring effect of the fibers on the deep soil structure. The enhanced interfacial force not only effectively transfers the load and redistributes the stress concentration but also prolongs the critical state of the soil body from strain intensification to softening, thus delaying the damage process of the specimen.

In terms of the number of cycles, the damage strain of the soil samples continued to decay as the number of dry and wet cyclic actions accumulated, and the deterioration rate increased significantly in the later stages of the cycle. This is due to the repeated inflow and outflow of water into and out of the soil under alternating wet and dry conditions, leading to its structural damage. The internal stresses generated in the soil due to hygroscopic expansion and dewatering contraction lead to microcracks between particles. These microcracks gradually expand and connect with each other, eventually forming a penetrating fracture network, which severely weakens the structural integrity and wholeness of the soil body [38]. At the same time, the penetrating moisture also weakened the bonding effect between the fibers and the soil body, which ultimately led to a sharp decrease in the mechanical properties of the specimens.

(2) Deformation modulus E_{50}

Table 7 summarizes the deformation modulus E_{50} determined from the stress-strain curves for different PVA fiber lengths, content amounts, and number of cycles.

Table 7. Modulus of deformation under dry and wet cycles (E_{50}).

Fiber length (FL) (mm)	Fiber content (FC) (%)	Number of cycles (N)	Deformation modulus (E_{50}) (MPa)
3	0.3	2	12.12
6			11.12
9			7.95
6	0.1	2	10.24
	0.3		12.06
	0.5		12.50
	0.8		12.94
3	0.3	2	11.67
		4	9.75
		6	8.47

The data in Table 7 show that the PVA fiber content in the wet and dry cycles showed a gain effect on the deformation modulus of the specimens, i.e., it increased with increasing content, which significantly enhanced their ability to resist deformation. However, the fiber length showed a negative effect, showing a significant decrease with the increase of fiber length. In particular, the deformation modulus peaked at a fiber length of 3 mm. This may be attributed to the fact that excessively long fibers tend to agglomerate or be unevenly distributed during the mixing process, which results in the inability to form a desirable stress structure within the soil. In addition, the deformation modulus of the specimens also decreased with the increase in the number of cycles, which indicated that the specimens were gradually subjected to microstructural damage during repeated wetting and drying processes.

3.1.2. Strength changes under wet and dry cycles

Figure 4 and Table 8 demonstrate the evolution of the unconfined compressive strength of the specimens undergoing wet and dry cycles for different variables.

Analysis of the data in Figure 4 and Table 8 shows that at constant fiber length and number of cycles, the uniaxial compressive strength of the specimens showed a nonlinear relationship with fiber content, which is shown by the fact that the strength of the soil samples increases and then decreases with the increase of fiber content. The compressive strength of the sample reaches its peak at a fiber content of 0.5%, with a compressive strength of 385.02 kPa, which is the optimal value among all mix designs. Compared with the plain soil samples, the strength loss values of soil samples at 0.1%, 0.3%, 0.5%, and 0.8% content were 19.93%, 18.79%, 17.53%, 8.36%, and 8.26%, respectively, which revealed that the increase in fiber content resulted in a significant decrease in the rate of strength loss. The reason lies in the fact that when the fiber content is below 0.5%, the insufficient fiber content makes it difficult to form an effective spatial reinforcement network. Consequently, the improvement in resistance to wet-dry cycling damage is limited, resulting in strength loss similar to that of the control group without fiber addition. When the fiber content was increased to 0.5%–0.8%, the fibers formed a stable reinforcing network, leading to a significant reduction in the rate of strength reduction in the

soil samples. The results indicate that a moderate increase in fiber content significantly enhances the ability of the specimens to inhibit the strength damage caused by alternating wet and dry cycles.

Table 8. Strength values under wet and dry cycling.

Fiber content (FC) (%)	Fiber length (FL) (mm)	Number of cycles (N)	UCS (kPa) Pre-cycle (kPa)	Post-cycle (kPa)	Absolute value (kPa)	UCS loss rate (%)
0.00	6	2	374.82	300.12	-74.70	-19.93
0.10			439.52	356.94	-82.58	-18.79
0.30			446.65	368.37	-78.28	-17.53
0.50			420.11	385.02	-35.09	-8.36
0.80			404.33	370.94	-33.39	-8.26
0.30	3	2	409.64	369.26	-40.38	-9.86
	6		386.72	338.43	-48.29	-12.49
	9		360.13	319.94	-40.19	-11.16
		0	370.20	370.20	0.00	00.00
0.30	3	2	386.23	357.75	-28.48	-7.38
		4	403.41	337.51	-65.90	-16.34
		6	427.23	228.54	-198.69	-46.51

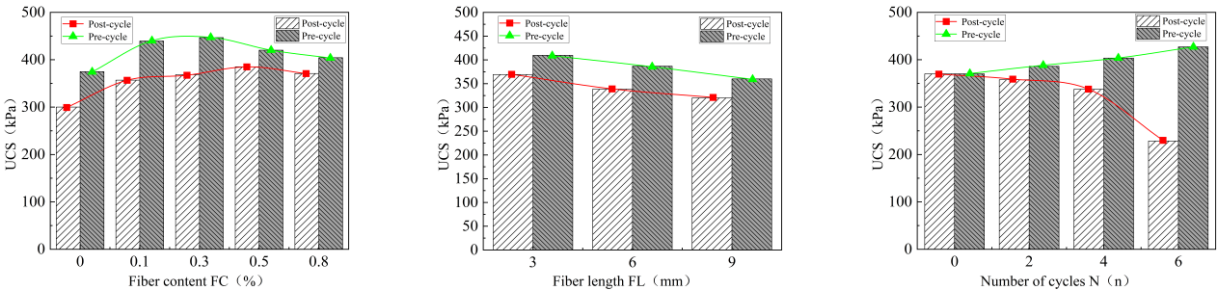


Figure 4. Variation of UCS under different variables.

At constant fiber content and number of cycles, the strength of the specimens was negatively correlated with the fiber length, and the increase in fiber length resulted in the attenuation of the uniaxial compressive strength of the specimens. The reduction in fiber compressive strength was 9.87%, 12.50%, and 11.14% for fiber lengths of 3, 6, and 9 mm, respectively. The main reason for this is that shorter fiber lengths are more likely to form a uniform isotropic distribution and effectively inhibit damage during the molding process, whereas longer fiber lengths may result in a reduction in structural strength due to the non-uniformity of the orientation arrangement. The rate of loss of uniaxial compressive strength in the tests was significantly less affected by changes in fiber length than by changes in fiber content, suggesting that the fiber length of the specimens has low sensitivity to wet and dry cycling.

In addition, the uniaxial compressive strength of the specimens produced significant cumulative damage as the number of cycles increased. The strength loss rate was 7.38% after 2 wet-dry cycles,

16.34% after 4 wet-dry cycles, and 46.50% after 6 wet-dry cycles. The principle of this deterioration lies in the fact that cycling intensifies the migration of free water within the soil, which in turn induces void formation [25]. With the increase in the number of cycles, the pores in the soil increased, particle migration and dissolution of the cementing phase accelerated, the damage of the soil material shifted toward brittle damage, and the damage of the specimen increased, resulting in a significant reduction in compressive strength.

3.1.3. Damage patterns under wet and dry cycles

Figure 5 shows the apparent morphology of the specimens after undergoing 2, 4, and 6 wet and dry cycles, in that order.

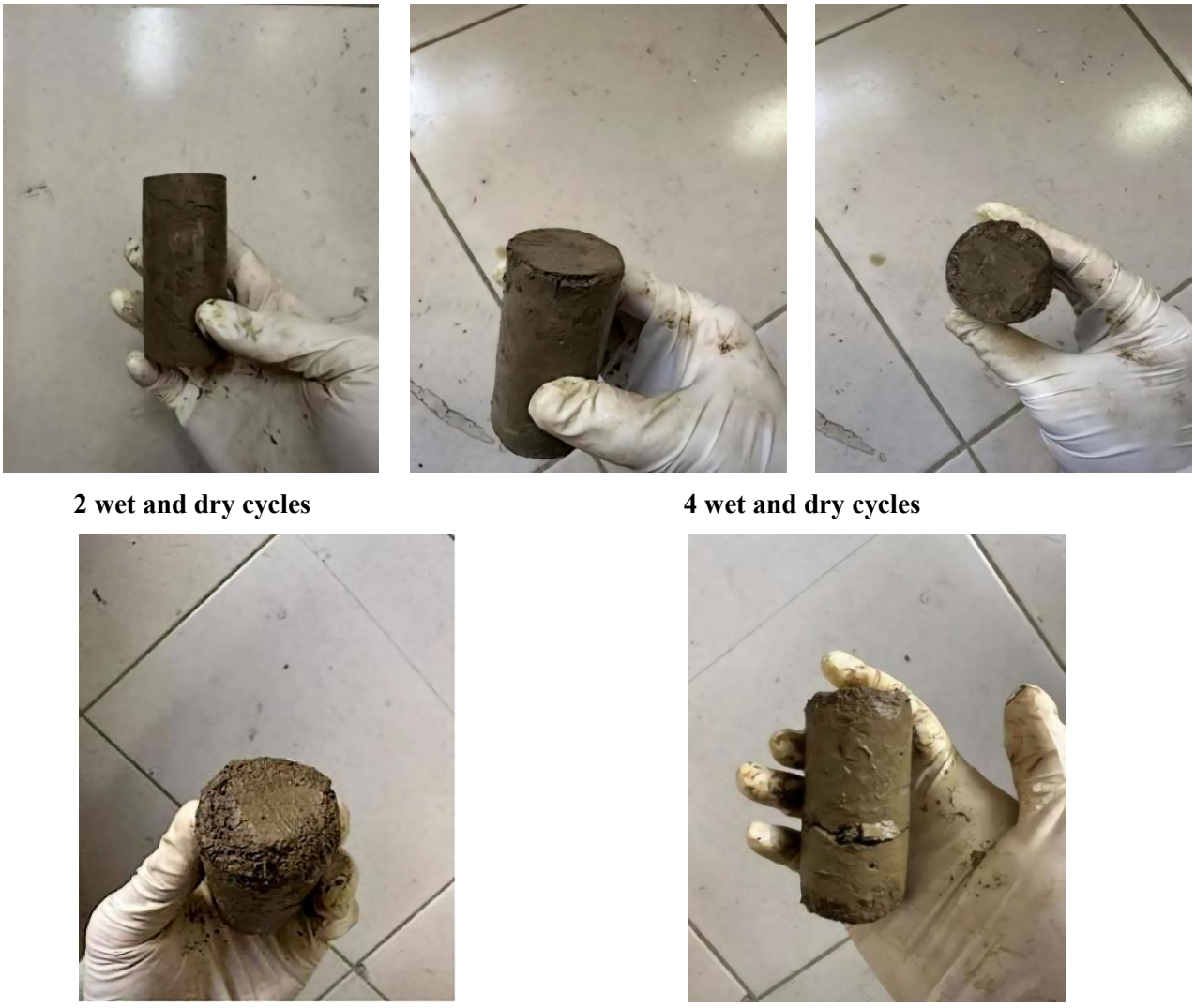


Figure 5. Damage patterns after different counts of wet and dry cycles.

From Figure 5, it can be seen that after two dry and wet cycles, only small cracks were observed on the surface of the specimen, which mainly resulted from the expansion and contraction effect triggered by the alternating dry and wet cycles, leading to the contraction of the soil body and

anisotropy. After four cycles, localized damage was observed on the top area of the specimen, accompanied by the spalling of part of the surface layer of the soil body. By the sixth cycle, significant development of cracks and serious structural damage were observed at the top edge area. As the cycle progressed to the sixth cycle, the surface of the specimen had formed significantly developed cracks, and the top edge area showed serious structural damage.

Under the action of wet and dry cycles, the key causative factor of specimen damage is the increase of water content inside the soil body due to the absorption of water, which triggers the increase of pore water pressure and thus the expansion pressure. As the water gradually fills the pore space, the cohesive force between soil particles is weakened. When the separation force exceeds the cohesive force, the particles are irreversibly separated, and the soil body is gradually loosened [38]. With the accumulation of the number of wet and dry cycles, the microfissures existing inside the specimen continuously sprout, expand, and penetrate each other under the action of cyclic stress and environmental factors (e.g., moisture migration, salt crystallization). This progressive damage accumulation process significantly weakened the integrity of the material and eventually triggered a sharp decrease in the unconfined compressive strength.

This study adopts the mass loss percentage to quantitatively assess the durability and failure resistance of soil samples under various variables, thereby reflecting their effectiveness against erosion and scouring. The mass loss percentage, denoted as Δ_i, is defined as the ratio of the mass lost by a soil sample after the testing process to its initial mass, typically expressed as a percentage (%). The calculation formula is:

$$\Delta_i = \frac{m_{i1} - m_{i0}}{m_{i0}} \times 100\% \tag{1}$$

In the formula, Δ_i represents the mass loss rate, m_{i0} denotes the mass of the soil sample before testing, m_{i1} indicates the mass of the soil sample after testing, and i signifies the test type, where $i = 1$ denotes the dry-wet cycle test, $i = 2$ denotes the freeze-thaw cycle test, and $i = 3$ denotes the sulfate resistance test.

For the three variables (fiber length, number of wet and dry cycles, and fiber content), Figure 6 presents the variation curves of the specimen mass under the corresponding conditions, respectively.

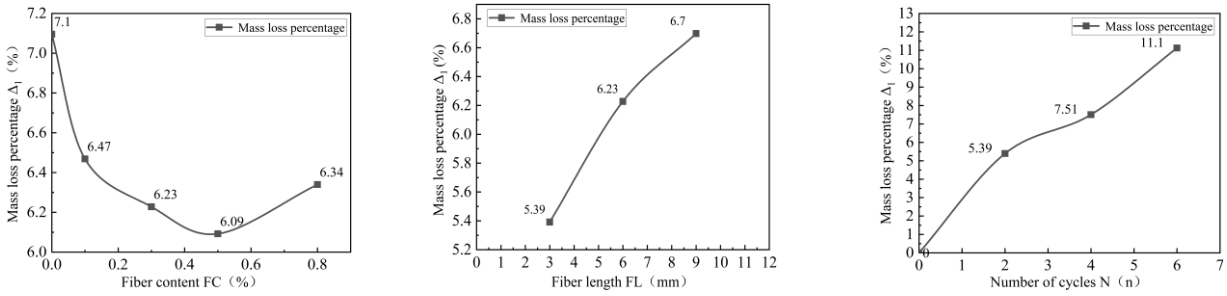


Figure 6. Mass loss rate for different cycle conditions.

As shown in Figure 6, the addition of PVA fibers significantly reduces the mass loss in wet and dry cycles, which is better than that of the fiber-free specimens. There is a non-monotonic relationship between the mass loss rate and the fiber content: as the PVA fiber content increases, the loss decreases

first, reaches a minimum value, and then increases and reaches a minimum value at 0.5% content. This is due to the lower content of fiber, fiber dispersion not being sufficient, and a local formation of stress concentration points, which results in higher porosity of the soil sample and a greater mass loss rate. The content of an appropriate amount of fiber can make the fiber network form an over-permeable structure, which can inhibit the penetration of the moisture migration path through the bridging effect, and cause the mass loss rate to plummet [39]. Regarding fiber length, the mass loss of the specimen increases with the increase of fiber length, mainly due to the exposure of more weak links of longer fibers in the tensile process, which leads to the increase of the probability of fiber rupture in the area of stress concentration, and thus produces more fracture debris resulting in mass loss [40]. With respect to the number of cycles, the increase in the number of wet and dry cycles resulted in a significant increase in the rate of mass loss of the specimens. The analyses showed that the mass loss rate was significantly affected by the number of cycles, particularly showing a marked increase from the fourth to the sixth cycle.

3.1.4. Shrinkage tests

Soils are subject to temperature and climate change, and they undergo a phase of water loss and drying. During this phase, the soil will continue to shrink and deform and, in extreme cases, may even be destroyed. In view of the potential hazards, the shrinkage index of a soil sample becomes a critical factor. To accurately collect the shrinkage index values of the samples, it is necessary to closely correlate the synergistic evolution of the sample volume and moisture content during the drying process. In practice, it is common to use the curve of line shrinkage versus water content to show the shrinkage characteristics of soil. To calculate the water content and line shrinkage at each point on the curve, the following formula is applied:

$$w_t = \left(\frac{m_t}{m_d} - 1\right) \times 100 \tag{2}$$

In which w_t is the specific moisture content of the soil sample at time t (%), and m_t is the specific mass of the soil sample at time t (g).

$$\delta_{st} = \frac{Z_t - Z_0}{h_0} \times 100 \tag{3}$$

In which δ_{st} is the soil sample line shrinkage (%) at moment t, Z_t is the reading at moment t (mm), and Z_0 is the initial reading (mm). The test is shown in Figure 7.

As can be seen from Figure 7, based on the curve characteristics, the soil shrinkage drying process can be divided into a constant velocity section (AB), a deceleration section (BC), and a residual section (CD). At the AB section, the line shrinkage rate decreases approximately linearly with the decrease of water content, reflecting a constant rate of water loss. When the water content decreases to a critical value, the rate of water evaporation from the soil body decreases and enters the BC deceleration stage, at which time the internal space of the soil body is gradually filled by void gas. Eventually, when the

water content tends to stabilize and enters the CD residual section, the soil body basically stops shrinking, and the evaporation process is close to completion.

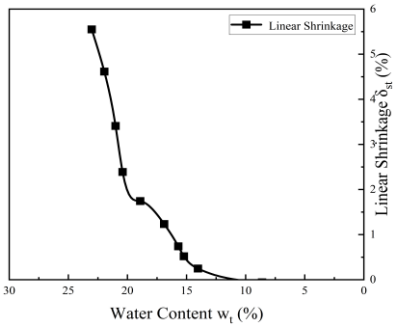


Figure 7. Moisture content–line shrinkage curve.

In addition, the linear relationship between shrinkage and moisture content can be fitted, and the results of the fit are shown in the equation in Figure 8:

$$\delta_s = aw^b \tag{4}$$

In which $R^2 = 0.99$, a = 5.38, and b = 5.81.

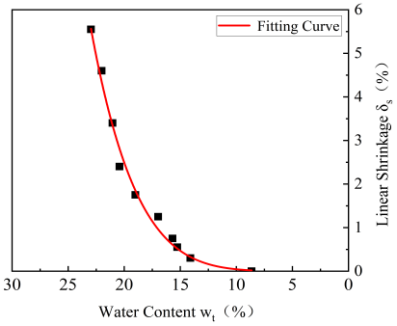


Figure 8. Linear shrinkage–moisture content fitting curve.

3.2. Freeze-thaw cycles

3.2.1. Stress-strain curves and deformation modulus

(1) Stress-strain curves

Figure 9 and Table 9 present the stress-strain curves of specimens of different variables under the action of freeze-thaw cycles.

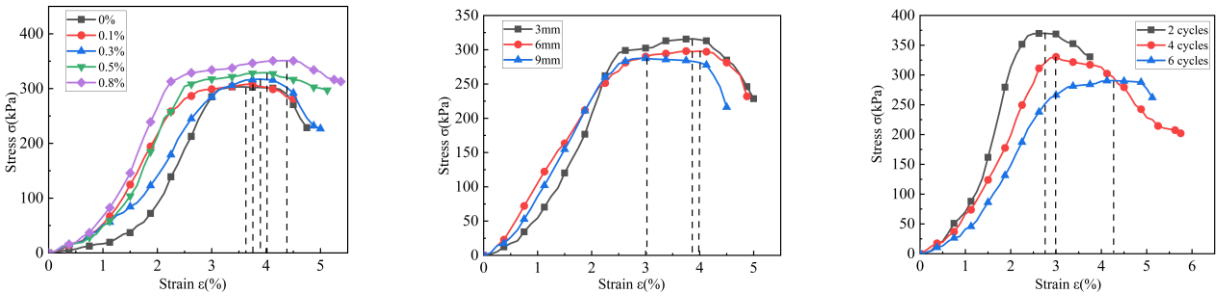


Figure 9. Stress-strain curves under different cycle conditions.

Table 9. Freeze-thaw cyclic failure strain (ε_f).

Fiber length (FL) (mm)	Fiber content (FC) (%)	Number of cycles (N)	Failure strain (ε_f)			
			Pre-cycle	Post-cycle	Absolute value	Rate of change (%)
3	0.3	2	3.86	3.79	-0.07	-1.81
6			3.94	3.91	-0.03	-0.76
9			4.15	3.11	-1.04	-25.06
6	0.1	2	3.66	3.60	-0.06	-1.64
	0.3		3.93	3.81	-0.12	-3.05
	0.5		4.30	3.90	-0.40	-9.30
	0.8		3.64	3.58	-0.06	-1.65
3	0.3	2	3.22	2.76	-0.46	-14.29
		4	3.98	3.72	-0.26	-6.53
		6	4.33	4.18	-0.15	-3.46

As shown in Table 9, at different dosage levels, the decrease in the failure strain with respect to the control group was 1.64%, 3.05%, 9.30%, and 1.65% when the content increased from 0.1% to 0.8%. The maximum decrease in the failure strain of the specimens was observed when the fiber content was 0.5%. In addition, the damage strain reduction of specimens caused by freeze-thaw cycles was slower than that of wet and dry cycles. The failure strength losses at different fiber lengths were as follows: 1.81% corresponding to 3 mm fibers, 0.76% corresponding to 6 mm fibers, and 25.06% corresponding to 9 mm fibers. Fibers of moderate length exhibit superiority in maintaining deformation resistance. The variation of failure strain at different numbers of cycles was a 14.29% reduction for 2 cycles, a 6.53% reduction for 4 cycles, and a 3.46% reduction for 6 cycles. Data shows that the breaking strain of the soil samples did not decrease continuously with the increase in the number of freeze-thaw cycles but rather increased gradually.

From Figure 9, it can be seen that the failure strain of the soil samples under freeze-thaw cycling continued to increase with the increase in fiber content, and this trend indicates that the effect of the deformation resistance of the specimens with the addition of PVA fibers was significantly improved under freeze-thaw cycling conditions. On the other hand, in terms of fiber length, the failure strain

increases and then decreases with the increase of fiber length, reaching a peak at a fiber length of 6 mm. In terms of the number of cycles, the failure strain increased with the increase of the number of cycles, which was mainly because the moisture in the soil would repeatedly freeze and thaw with the freeze-thaw cycle; this repeated change would cause the extrusion and abrasion of the soil particles, which eventually led to the substantial damage of the specimens.

(2) Deformation modulus E_{50}

Based on the stress-strain curve analysis, the deformation modulus data were obtained for different variables and content levels, and the specific values are summarized in Table 10.

Table 10. Freeze-thaw cycle modulus of deformation (E_{50}).

Fiber length (FL) (mm)	Fiber content (FC) (%)	Number of cycles (N)	Deformation modulus (E_{50}) (MPa)
3	0.3	2	11.29
6			11.49
9			11.54
6	0.1	2	10.31
	0.3		11.28
	0.5		11.38
	0.8		13.58
3	0.3	2	12.36
		4	10.63
		6	9.06

Table 10 shows that increasing the fiber content significantly increases the modulus of deformation of the specimens, indicating the effectiveness of fibers in improving freeze-thaw deformation resistance. The effect of fiber length is relatively weak: although the modulus increases slightly with length, the modulus values are close to each other at all lengths, suggesting a limited effect on the freeze-thaw deformation modulus. In addition, as the number of freeze-thaw cycles increases, the measured deformation modulus shows a decreasing trend, which is attributed to the cyclic damage that reduces the deformation resistance of the soil structure.

3.2.2. Strength changes under freeze-thaw cycles

The changes in the unconfined compressive strength of specimens of different variables under freeze-thaw cycles and the quantitative data are detailed in Figure 10 and Table 11.

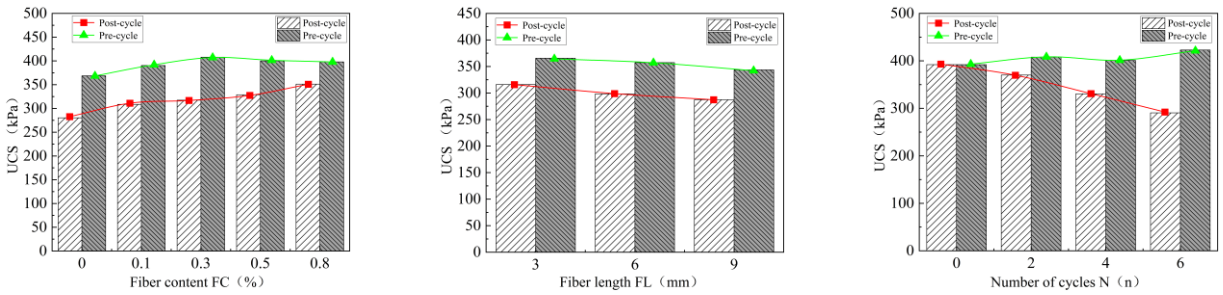


Figure 10. Variation of unconfined compressive strength under different variables.

Figure 10 and Table 11 show that the inclusion of fibers resulted in good freeze-thaw resistance of the specimens under freeze-thaw cycles. Under the premise that the number of freeze-thaw cycles and fiber length were kept constant, the uniaxial compressive strength of the specimens was positively correlated with the fiber content: the strength of the soil samples increased with the increase in fiber content. Specifically, the percentage decrease in strength at different fiber contents was 23.98%, 22.19%, 20.93%, 17.83%, and 11.78%, respectively. This indicates that as the fiber content gradually increases, the strength loss rate shows a decreasing trend. Particularly when the content reaches 0.8%, the control effect on strength loss becomes more pronounced. This demonstrates that the incorporation of fibers plays a positive role in enhancing the freeze-thaw resistance of soil samples.

Table 11. Strength values under freeze-thaw cycles.

Fiber content (FC) (%)	Fiber length (FL) (mm)	Number of cycles (N)	UCS (kPa) Pre-cycle (kPa)	Post-cycle (kPa)	Absolute value (kPa)	UCS loss rate (%)
0.00	6	2	368.61	280.23	-88.38	-23.98
0.10			407.83	317.33	-90.50	-22.19
0.30			390.22	308.54	-81.68	-20.93
0.50			400.01	328.72	-71.29	-17.83
0.80			398.04	351.16	-46.88	-11.78
0.30	3	2	365.62	315.93	-49.69	-13.59
	6		357.24	298.34	-58.90	-16.49
	9		343.65	287.46	-56.19	-16.36
0.30	3	0	392.00	392.00	0.00	0.00
		2	407.81	370.03	-37.78	-9.27
		4	400.85	330.56	-70.29	-17.54
		6	422.83	290.54	-132.29	-31.29

When the number of cycles and fiber content were kept constant, the strength of soil samples weakened with the increase in fiber length. The strength loss rates corresponding to different fiber lengths were 13.59%, 16.49%, and 16.36%, and the change of strength loss rate with fiber length was not significant, indicating that the fiber length had a limited effect on the freeze-thaw resistance of the

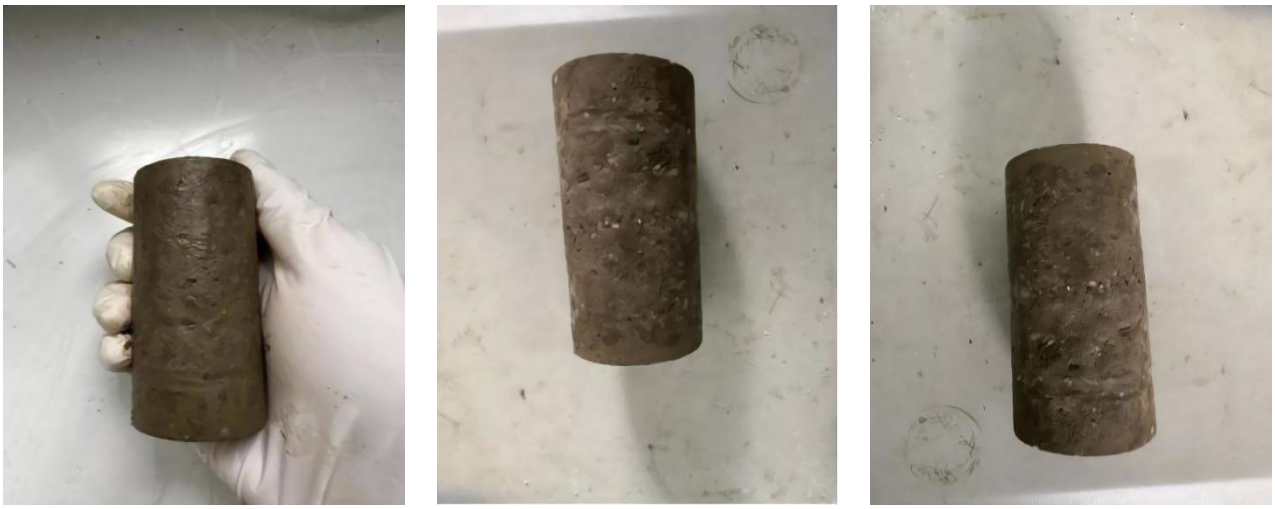
specimens.

Under the freeze-thaw cycle, when the fiber length and fiber content were kept constant, the strength of the specimens showed a significant decay trend, and the rate of strength loss increased sharply with the increasing number of cycles. Specifically, 2, 4, and 6 cycles corresponded to a strength loss of 9.27%, 17.54%, and 31.29%, respectively. This deterioration is attributed to the moisture phase change induced by freeze–thaw cycling: when the water in the soil freezes, it expands in volume and thus exerts failure stresses on the soil structure. After several freeze-thaw cycles, the continuous expansion force leads to irreversible damage in the soil [41]. At the same time, microcracks gradually develop and expand through the soil body, eventually leading to structural instability and damage.

3.2.3. Damage patterns under freeze-thaw cycles

Figure 11 shows the damage morphology of the specimens under freeze-thaw conditions for 2, 4, and 6 freeze-thaw cycles, respectively.

As can be seen from Figure 11, no discernible cracks, damage, or structural damage were detected in the specimens during the entire freeze-thaw cycle test. The principle of freeze-thaw cycling lies in the repeated ice-water phase transition of water molecules inside the specimens and their accompanying migration in the pores. It is this internal water state change and migration process that is the root cause of the microstructural reconfiguration of lightweight soils, which in turn leads to changes in their macroscopic physical and mechanical properties [42].



2 freeze-thaw cycles **4 freeze-thaw cycles** **6 freeze-thaw cycles**

Figure 11. Damage patterns after different counts of freeze-thaw cycles.

Figure 12 shows the variation curves of the mass of the specimens for different numbers of cycles, fiber length, and fiber content.

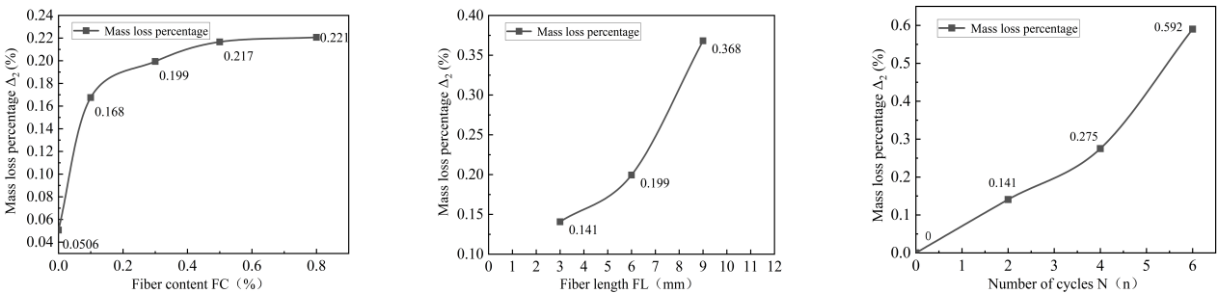


Figure 12. Mass loss rate for different cycle conditions.

Figure 12 indicates that the mass of specimens decreases with increasing fiber content, fiber length, and freeze-thaw cycle count. Regarding the effects of fiber content and length, the mechanism is as follows: when fiber content is low or fiber length is insufficient, fibers struggle to form a continuous and effective spatial reinforcement network within the soil matrix. During freeze-thaw cycles, soil particles absorb water and expand, potentially causing a temporary increase in specimen mass during the initial stages. However, once fiber content and length reach a certain threshold, the fibers' restraining and bridging effects gradually become dominant. This effectively suppresses the soil's water absorption and expansion, resulting in a sustained decrease in specimen mass as freeze-thaw cycles progress. It should be emphasized that, due to the current lack of available microstructural images, the above explanation regarding the formation of the fiber spatial structure and its confinement mechanism remains a hypothetical inference based on experimental phenomena. Its specific micro-mechanism requires further verification through methods such as microscopic observation or microscale numerical simulation in the future. Additionally, as the number of freeze-thaw cycles increases, the specimen mass continues to decrease due to the gradual spalling of surface material, but the cumulative mass loss rate throughout the entire test process remains low.

3.3. Resistance to sulfate

3.3.1. Stress-strain curves and deformation modulus

(1) Stress-strain curves

The stress-strain curves of the specimens under sulfate exposure for different variables are shown in Figure 13, and specific values are in Table 12.

Table 12. Failure strain against salt stress (ε_f).

Fiber length (FL) (mm)	Fiber content (FC) (%)	Number of cycles (N)	Failure strain (ε_f)			
			Pre-cycle	Post-cycle	Absolute value	Rate of change (%)
3	0.3	2	3.72	4.73	1.01	27.15
6			3.80	4.89	1.09	28.68
9			4.02	5.11	1.09	27.11
6	0.1	2	3.52	4.31	0.79	22.44
	0.3		3.79	4.43	0.64	16.89
	0.5		4.21	4.96	0.75	17.81
	0.8		4.40	5.00	0.60	13.64
3	0.3	2	3.81	4.25	0.44	11.55
		4	3.95	4.35	0.40	10.13
		6	—	—	—	—

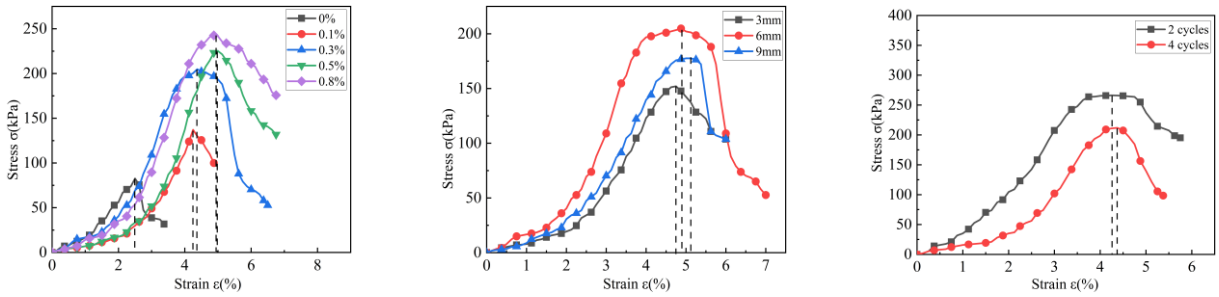


Figure 13. Stress-strain curves under different cycle conditions.

Analyzing the data in Table 12, it was found that the damage strain of the experimental group is significantly higher than that of the control group in the salt cycling environment. This is maybe because the crystallized substances formed on the specimen surface during salt immersion can fill the microcracks and slow down the process of crack expansion. At the same time, the fibers can inhibit the development of crack penetration through the three-dimensional mesh structure, and the PVA fibers can improve the ductility of the soil body and increase the damage strain of the specimen before the damage occurs. The variation in damage strain increases the rate of specimens with different fiber content: 0.1% fiber content corresponds to 22.44%, 0.3% fiber content corresponds to 16.89%, 0.5% fiber content corresponds to 17.81%, and 0.8% fiber content corresponds to 13.64%. As shown in Table 12, when the fiber content is within the range of 0.5%–0.8%, the specimens exhibit higher post-cycle strain and improved ductility, indicating that a higher fiber content provides more effective restraint on crack propagation and significantly enhances the material's toughness and energy dissipation capacity.

At different lengths, the increase in failure strain measured at different fiber lengths is as follows: 27.15% for 3 mm fiber length, 28.68% for 6 mm fiber length, and 27.11% for 9 mm fiber length, with

similar increases in failure strain for soil samples, indicating that the change in fiber length has limited influence on the failure strain of the specimens in the sulfate-aggressive environment. In terms of the number of cycles of salt resistance, the growth rate of failure strain was 11.55% in 2 cycles, and 10.13% in 4 cycles; specimens were severely damaged in 6 cycles, thus losing the bearing capacity, and it was not possible to accurately measure the corresponding data, which indicated that the number of cycles had a significant effect on the damage of specimens under the condition of sulfate erosion.

From Figure 13, it can be seen that fiber content can effectively increase the failure strain of the specimens, increase the ductility of the soil specimens, and slow the failure process compared with the undoped specimens. In terms of fiber content, the failure strain of the specimen doped with 0.8% was about twice that of the undoped specimen, showing an obvious enhancement effect. In terms of fiber length, an increase in fiber length increases the failure strain of the specimens, but the increase is not significant, reflecting the low contribution of this parameter to the saltwater permeability resistance. In terms of the number of cycles, the failure strains of the specimens were closer after 2 and 4 cycles, and after 4 cycles, the specimens showed obvious brittle damage.

(2) Deformation modulus (E_{50})

Based on the stress-strain curve analysis, the values of deformation modulus E50 were determined for different variables, and the main relevant parameters are summarized in Table 13.

Table 13. Failure strain against salt stress (ε_f).

Fiber length (FL) (mm)	Fiber content (FC) (%)	Number of cycles (N)	Deformation modulus (E_{50}) (MPa)
0.10	6	2	2.51
0.30			4.32
0.50			4.41
0.80			4.55
0.30	3	2	3.81
	6		4.23
	9		4.38
0.30	3	2	4.23
		4	3.27
		6	–

Analysis of the data in Table 13 shows that the modulus of deformation of the specimens continues to increase in the salt environment with increasing PVA fiber content. For fiber length, specimens with longer fibers exhibited higher deformation modulus, likely because longer fibers can sustain greater tensile strains under salt conditions by bridging and inhibiting microcrack propagation. However, irrespective of content or length, these improved effects were significantly weakened at lower PVA content, resulting in an overall decrease in the deformation modulus. At the same fiber content and length, the deformation modulus of the specimens decreases progressively as the number of cycles increases.

3.3.2. Strength changes under sulfate stress

The variation of the unconfined compressive strength of the specimens under sulfate stress for different variables is shown in Figure 14, and specific values are given in Table 14.

Table 14. Salt resistance values.

Fiber content (FC) (%)	Fiber length (FL) (mm)	Number of cycles (N)	UCS (kPa) Pre-cycle (kPa)	Post-cycle (kPa)	Absolute value (kPa)	UCS loss rate (%)
0.00			237.21	82.62	-154.59	-65.12
0.10			247.95	137.15	-110.80	-44.70
0.30	6	2	281.33	204.84	-76.49	-27.20
0.50			275.51	225.00	-50.51	-18.33
0.80			270.72	242.63	-28.09	-10.38
	3		366.61	152.10	-214.51	-58.51
0.30	6	2	357.25	204.84	-152.41	-42.67
	9		323.63	177.65	-145.98	-45.12
		0	266.32	266.32	0.00	0.00
		2	298.03	211.84	-86.19	-28.93
0.30	3	4	316.41	123.11	-193.30	-61.09
		6	—	—	—	—

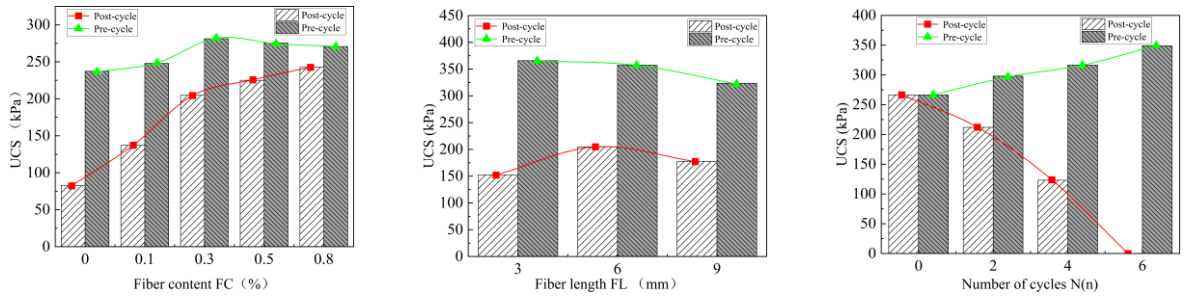


Figure 14. Variation of unconfined compressive strength under different variables.

From Figure 14 and Table 14, it can be seen that the strength loss rates corresponding to different fiber content varied: 0.1% fiber content corresponded to 44.70%, 0.3% fiber content corresponded to 27.20%, 0.5% fiber content corresponded to 18.31%, and 0.8% fiber content corresponded to 10.38%. It can be seen that the strength loss rate shows a significant decreasing trend with the increase in fiber content, which indicates the role of fiber in suppressing strength deterioration and strengthening the ability of the specimens to resist salt erosion. This phenomenon is mainly attributed to the inherent erosion resistance of PVA fibers, which can form a bridging structure inside the soil body. This structure can effectively restrain the generation and extension of cracks and block the infiltration channels of erosion ions, which ultimately enhances the overall erosion resistance of the material.

The results indicate that the influence of fiber length on the specimen strength shows an initial

increase followed by a decrease. The 6 mm fibers yielded the highest compressive strength and the lowest strength loss rate (42.66%), outperforming those of 3 mm fibers (58.41%) and 9 mm fibers (45.12%). This behavior may be attributed to a more effective crack-bridging mechanism provided by the 6 mm fibers, which is consistent with conclusions reported in previous studies by Ning et al., Wu et al., and Xie et al. [43–45]. In contrast, 3 mm fibers are too short to adequately bridge and arrest cracks, whereas 9 mm fibers are prone to entanglement or agglomeration during mixing, reducing their reinforcing efficiency. The intermediate 6 mm fiber length theoretically achieves a balance between effective crack bridging and uniform dispersion, thereby offering an optimal bridging effect. It should be noted that the mechanism underlying this presumed optimal bridging behavior at the microscale remains hypothetical and requires further validation through microscopic observations and mesoscale numerical simulations.

In terms of the number of cycles, with the increase of the number of freeze-thaw cycles, the strength of the specimens showed an obvious deterioration trend, with a 28.90% decrease in strength after two cycles and a 61.11% decay of the specimen's strength after experiencing four salt-aggression cycles. Specimens were destroyed after 6 cycles. The main reason for the deterioration is that the cement hydration products will react chemically with corrosive ions, and the continuous accumulation of their reaction products not only fills the specimen pores but also induces the generation of microcracks [46]. As the erosion cycle advances, the products gradually occupy the pore space and microcrack space, and under the action of internal stress, the original microcracks can be expanded and form larger cracks. This degradation process eventually leads to a sharp decrease in the ability of the PVA fiber soil to resist salt erosion, and the rate of strength loss increases.

3.3.3. Damage patterns under sulfate stress

Figure 15 shows the morphology of the specimens after two, four, and six cycles of sulfate erosion.



Figure 15. Damage patterns for different numbers of sulfuric acid erosion cycles.

As can be seen from Figure 14, after two cycles, the surface of the specimen was obviously spalled, but the overall structure was still intact. After four cycles, the surface of the specimen was covered

with a large number of white salt precipitates, and an obvious crack network was formed. After the sixth cycle, the structure of the specimen failed completely, manifested by the surface layer of the soil body being dislodged in patches, and significant through-fracture was developed in the internal part of the specimen. This damage process is attributed to the expansion of the pores in response to the continuous swelling force, which constitutes the core mechanism of the damage process by progressively damaging the soil microstructure and ultimately leading to the deterioration of the overall strength [47]. Chloride and sulfate ions erode the soil skeleton during prolonged immersion, thus inevitably reducing the unconfined compressive strength of the specimens. At the initial stage of specimen immersion, salts accumulate and crystallize within the pores, and the crystallization fills some of the micropores of the soil, so that the decrease in strength of the lightweight soil is relatively slow. However, with prolonged immersion, salt crystals continue to be generated on the surface and in the pores of the soil samples, which generate significant expansion stresses that will gradually destroy the internal structure of the samples, ultimately leading to the loss of structural integrity of the samples and a significant decrease in strength.

Figure 16 shows the variation curves of specimen mass under sulfate stress for different numbers of cycles, fiber content, and fiber length.

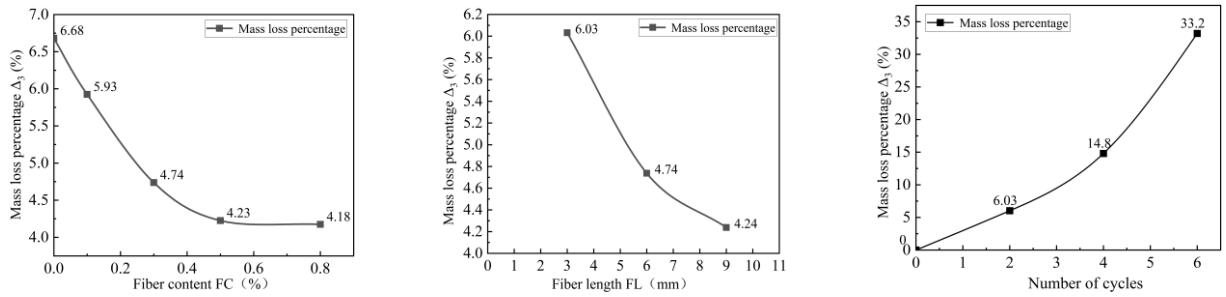


Figure 16. Mass loss rate for different cycle conditions.

As can be seen from Figure 16, the introduction of PVA fibers significantly reduces the mass loss rate of the specimens compared to the unadulterated specimens, and the increase in the content and length of PVA fibers contributes to the reduction of the mass loss of the specimens. However, the accumulation of the number of freeze-thaw cycles significantly amplified the mass loss effect, as shown by the increase in the loss rate with the increase in the number of cycles.

3.4. Scour resistance test

The equipment and procedures for scour resistance testing are relatively complex and time-consuming. Conducting scour resistance tests for every initial mix design would involve a substantial workload and would be extremely time-consuming. When the fiber content is 0.3% and the fiber length is 3 mm, the unconfined compressive strength of the soil sample reaches its peak value. Therefore, this group was selected as the subject for scour resistance testing to evaluate the scour resistance performance of PVA-reinforced silt under optimal modification conditions. Figure 17 shows the unflushed graph and the changes after 2, 6, 8, and 12 h of flushing.

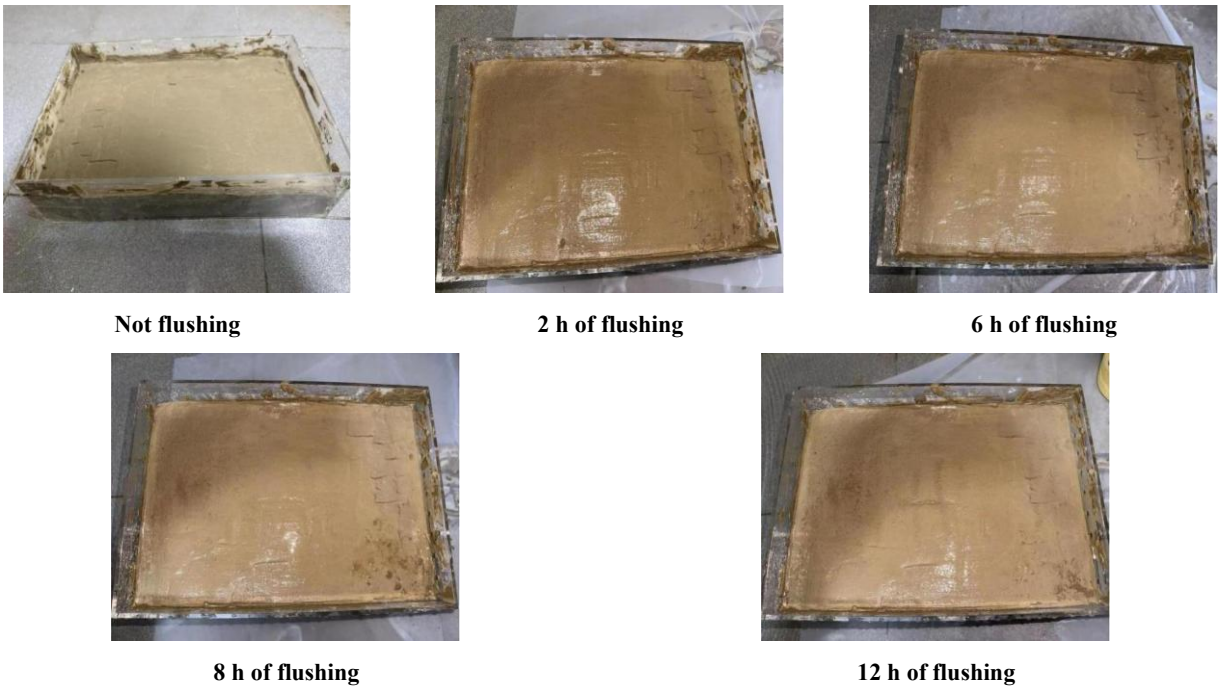


Figure 17. Scour plots of specimens at different time intervals.

As can be seen from Figure 17, the surface condition of the specimens changed significantly under different scouring durations. Within the first 6 h of flushing, the surface of the specimen showed no significant flushing marks compared with the initial state. However, at this stage, more scratches appeared on the specimen surface. This was mainly due to the loss of inhomogeneous soil particles on the specimen surface under water scouring. As the scouring time increased to 8 h, there were still no visible signs of damage on the specimen surface, but a noticeable accumulation of clay particles appeared at the bottom of the sample. However, localized photographs after 12 h showed a large number of micropores on the surface of the specimen compared to the original state. This was attributed to the longer time the specimen was immersed in water and the gradual penetration of water into the interior of the specimen.

In this study, the scour rate was chosen to assess the effectiveness of slope scour resistance, which is the ratio of the dried mass of scour-lost soil to the initially dry soil mass of the transparent soil box. Figure 18 shows the scour rate W_a, which is calculated by the formula:

$$W_a = \frac{\Delta m}{m_s} \times 100\% \tag{5}$$

In the formula, W_a is the scouring rate, Δm is the mass of soil sample lost due to scouring, and m_s is the initial mass of the soil sample before scouring.

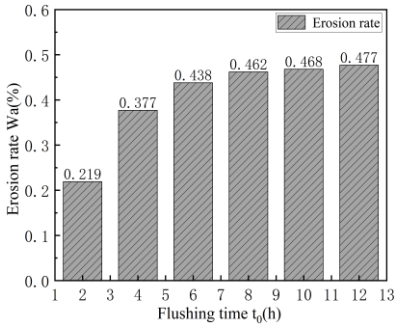


Figure 18. Flushing rate chart.

As shown in Figure 18, the scour resistance of the specimens exhibits a pronounced nonlinear decay characteristic with flushing time (t_0). The variation of the corresponding scour rate of the specimens at each time point was as follows: 0.219% for 2 h, 0.376% for 4 h, 0.438% for 6 h, 0.462% for 8 h, 0.468% for 10 h, and 0.472% for 12 h. The growth rates corresponding to the erosion rates W_a were 0.157%, 0.061%, 0.023%, 0.006%, and 0.005% for each 2-h period. From the data, it can be seen that although the scour rate continues to increase with time, its increment decreases step by step, indicating that the specimen has good resistance to scour, given that the scour rate is below 0.5% within 12 h and grows slowly in the later stages. This rapid decay of the scour rate indicates the formation of an effective scour resistance mechanism on the surface of the material, with the PVA fibers inhibiting crack extension and delaying the spalling of the matrix material through a bridging effect [48].

Although the laboratory tests in this study were conducted under strictly controlled conditions, the soft soil types and field environments encountered in actual engineering applications are far more complex, which may lead to discrepancies in the performance of fiber-reinforced soils. Therefore, the limitations of the experimental setup and the potential influence of soft soil types on the test results must be discussed, which are mainly reflected in the following aspects:

(1) The tests (wet-dry, freeze-thaw, salt erosion cycles, and scouring tests) conducted in this study were carried out under relatively stable and controlled conditions. However, in real engineering environments, factors such as temperature, humidity, salinity, and water flow velocity can fluctuate considerably with seasonal and climatic changes, potentially leading to long-term degradation behaviors that differ from those observed in laboratory settings. Moreover, while the specimens in the experiments experienced relatively uniform stress states, soils in actual engineering applications are influenced by multiple external factors such as complex load transfer, variable boundary conditions, and ground settlement. These factors may lead to mechanical responses of fiber-reinforced soils that do not fully align with laboratory results. Furthermore, although laboratory conditions ensure uniform mixing of soil and fibers, in situ soils typically exhibit complex compositions, and variations in compaction quality or environmental disturbances during construction may also affect the reinforcing performance of PVA fibers.

(2) Due to constraints imposed by experimental conditions, it is challenging to fully simulate the cumulative damage effects observed during long-term service. In field environments, soil subjected to years of freeze-thaw cycles or repeated wetting and drying may exhibit more pronounced structural degradation. It is recommended to combine short-term accelerated indoor aging tests (freeze-thaw, moisture, salt exposure, fatigue, and creep) with long-term in situ monitoring, microscopic

characterization, and numerical life prediction. This integrated approach enables systematic evaluation of the long-term durability of PVA fiber-reinforced soils and establishes reliability boundaries for engineering applications in the future.

(3) Different soft soils may influence the long-term durability test results. Soft soils with high clay content or a high plasticity index are prone to greater volume changes, pronounced crack development, and rapid structural deterioration under wet-dry and freeze-thaw actions, leading to more marked strength reduction. The initial moisture content, compactness, and consistency of soft soils also directly affect their degradation under cyclic or erosive conditions. Furthermore, differences in microstructure and cementation properties (such as natural structure, organic matter content, and soluble salt content) can lead to distinct failure modes under sulfate erosion and scouring.

4. Conclusions

In this study, the erosion resistance of PVA fiber-reinforced mucky clay was systematically evaluated with the help of wet-dry cycles, freeze-thaw cycles, salt erosion, and scour tests. During the wet-dry cycling phase, the addition of fibers effectively improved the deformation characteristics of the soil. As the fiber content increased, both ductility and failure strain showed a gradual strengthening trend. When the fiber content reached 0.5%–0.8%, the specimens exhibited outstanding toughness characteristics and significant failure strain. The unconfined compressive strength of PVA fiber-reinforced soils undergoing wet and dry cycling showed a nonlinear increasing trend and then decreased with fiber content. Compared with the effect of the length of PVA fibers, the effect of the added dosage on the enhancement of dry and wet cycling stability was more significant. During the shrinkage process of soil samples, sample shrinkage experienced three stages: constant rate, deceleration rate, and residual. Under freeze-thaw cycles, fiber incorporation significantly increased the compressive strength of the samples. However, the strength loss rate showed little variation with fiber length, indicating that fiber length had a limited effect on freeze-thaw resistance. Under the salt immersion test, the specimen strength increased with higher fiber content, and the strength loss rate decreased markedly as the content increased. However, variations in fiber length had no evident effect on the improvement in the salt-erosion test. The scour resistance test results indicated that the erosion rate remained at a very low level, demonstrating that the specimens possessed excellent erosion resistance.

Use of AI tools declaration

The authors declare they have not used Artificial Intelligence (AI) tools in the creation of this article.

Acknowledgments

All authors (Y.X.W., J.H.G. and K.Y.C) contributed to the conceptualization and writing of the original draft, as well as reviewed and carried out the final editing of this manuscript.

Conflict of interest

The authors declare no competing interests.

References

1. Shen Zhujiang (1998) Engineering Characteristics of Soft Soil and Design of Soft Soil Foundation. *Chin J Geotech Eng* 01: 100–111.
2. Kang Chenglei, Lin Wenquan (2015) Research on Disease Prevention of Bridge Engineering in Deep Soft Soil Area. *J Railway Eng* 32: 73–78.
3. Yan Zhen ying (2019) Soft Soil Foundation Problems and Treatment Techniques in Highway Engineering Construction. *China Highway* 2: 114–115. DOI: 10.13468/j.cnki.chw.2019.02.038.
4. CHA Fusheng, LIU Jingjing, HAO Ailing, et al. (2015) Experimental study on strength and microscopic properties of cement-cured lead-contaminated soil under NaCl erosion environment. *J Rock Mech Eng* 34: 4325–4332. DOI: 10.13722/j.cnki.jrme.2014.0929.
5. FIRAT O E M (2017) Research on Thermal and Mechanical Properties of Fiber Reinforced Soil. Beijing Jiao tong University, 2017.
6. Tao Yingyang (2014) A Brief Analysis of the Future Development Direction of PVA Fibers. *High-tech Fiber Appl* 39: 34–37.
7. Liu Yan Ning, Zhang Tao, Li Shan (2022) Experimental Study on Mechanical Properties of Cement-based Composite Materials Mixed with Fine Steel Fiber/PVA Fiber. *Concrete* 2022: 112–115.
8. Zheng Rui (2021) Research on Mechanical Properties and Chloride Ion-Resistant Erosion Resistance of PVA Fiber-impregnated Granular Concrete. Jilin University, 2021.
9. Zhang Peng, Li Chen-di, Wang Juan, et al. (2021) Synergistic reinforcement of nano-SiO2 and PVA fibers in concrete for improving mechanical properties. *Highway* 66: 271–275.
10. Ramesh Talreja (2014) Assessment of the fundamentals of failure theories for composite materials. *Compos Sci Technol* 105: 190–201. https://doi.org/10.1016/j.compscitech.2014.10.014
11. Ding J, Ma D, Zhang R, et al. (2025) Investigating on dynamic and static mechanical characteristics and microscopic mechanism of fiber-reinforced and rubberized cement stabilized soil under dry-wet cycle sulfate erosion. *Constr Build Mater* 487: 142083. https://doi.org/10.1016/j.conbuildmat.2025.142083
12. Rawat V, Satyam N (2024) Enhancing the durability of coastal soil treated with fiber-reinforced microbial-induced calcite precipitation (MICP). *Appl Ocean Res* 150: 104106. https://doi.org/10.1016/j.apor.2024.104106
13. Shettigar S, Gowrishankar M C, Shettar M (2025) Review on aging behavior and durability enhancement of bamboo fiber-reinforced polymer composites. *Molecules* 30: 3062. https://doi.org/10.3390/molecules30153062
14. Zhang P, Li Q, Wang J, et al. (2019) Effect of PVA fiber on durability of cementitious composite containing nano-SiO2. *Nanotechnol Rev* 8: 116–127. https://doi.org/10.1515/ntrev-2019-0011
15. Lei B, Pang S, Sun J, et al. (2025) Rheological Properties and Freeze-Thaw Durability of Fiber-Reinforced Flowable Solidified Soil Incorporating Multi-Source Waste. *Results Eng* 2025: 107892. https://doi.org/10.1016/j.rineng.2025.107892

16. Zeng Y, Peng L, Ma B, et al. (2025) Influence of multi-walled carbon nanotubes on the performance of nano-silica enhanced lightweight cement-based composites under cyclic action of freeze-thaw and erosion. *Constr Build Mater* 493: 143132. https://doi.org/10.1016/j.conbuildmat.2025.143132
17. Zeng Y, Li X, Tang A, et al. (2023) Axial compressive behavior of basalt and polyacrylonitrile fibers reinforced lightweight aggregate concrete with industrial waste ceramsite-Lytag after freeze-thaw cycles. *J Build Eng* 76: 107402. https://doi.org/10.1016/j.jobe.2023.107402
18. Qu W, Maimt N, Qu J (2025) Effects of zeolite and palm fiber on the weathering resistance and durability characteristic of cement soil. *Sci Rep* 15: 4408. https://doi.org/10.1038/s41598-025-88841-4
19. Dhakal S, Kolay P, Puri V (2024) Durability of clayey soil stabilized with calcium sulfoaluminate cement and polypropylene fiber under extreme environment. *Transp Geotech* 44: 101164. https://doi.org/10.1016/j.trgeo.2023.101164
20. Youn I, Bang S, Jeong Y, et al. (2023) Evaluating the Strength and Durability of Eco-Friendly Stabilized Soil Bricks Incorporating Wood Chips. *Appl Sci* 13: 10929. https://doi.org/10.3390/app131910929
21. Liang Z, Yan C, Cao Y, et al. (2025) Influence of dry-wet cycles on the strength behavior of biopolymer and fiber composite modified loess. *J Mater Res Technol* 2025. https://doi.org/10.1016/j.jmrt.2025.07.071
22. Wan L, Zhao Y, Yu M, et al. (2024) Durability and Mechanical Properties of Nano-SiO2 and Polyvinyl Alcohol Fiber-Reinforced Cementitious Composites Subjected to Saline Freeze–Thaw Cycles. *Materials* 17: 2542. https://doi.org/10.3390/ma17112542
23. Zhang P, Sun X, Wei J, et al. (2023) Influence of PVA fibers on the durability of cementitious composites under the wet–heat–salt coupling environment. *Rev Adv Mater Sci* 62: 20230155. https://doi.org/10.1515/rams-2023-0155
24. Yan Changwang, Cao Yunfei, Liu Shuguang, et al. (2020) Experimental study on salt erosion resistance of PVA fiber concrete. *Concrete* 2020: 56–60.
25. MA Nan, WANG Lin, LI Yingle (2021) Experimental study on sulphate erosion resistance of PVA fiber-reinforced concrete under dry and wet alternation mechanism. *China Test* 47: 142–147.
26. ZHAO Xiaoming, WANG Xinke, QIAO Hongxia, et al. (2022) Study on the damage law and model of freeze-thaw cycle of PVA fiber concrete. *Concr Cem Prod* 2022: 53–57.
27. Tan H, Ma C, Li S, et al. (2024) Experimental study on the influence of fiber characteristics on the working property of underwater flowable solidified soil: Flowability, anti-dispersion, strength and anti-scour resistance. *Ocean Eng* 312: 119230. https://doi.org/10.1016/j.oceaneng.2024.119230
28. Li L, Li S, Li W, et al. (2025) Mechanical properties of soil reinforced by fiber and alkaline-activated rice husk ash, and rainfall erosion model tests. *Sci Total Environ* 958: 178099. https://doi.org/10.1016/j.scitotenv.2024.178099
29. National Standard of the People's Republic of China. GB/T 50123-2019, Standard for geotechnical testing method. Beijing: China Planning Press, 2019.
30. ZHU Dinghua, DONG Leiping, HE Feng, et al. (2010) Compressive strength characteristics of lightweight mixed soil with polystyrene fiber. *J Nanjing Univ Technol* 32: 53–57.
31. Wang Lu-ming, wang di-fei (2015) Experiments and research on promoting the agglomeration and hardening of cement foam concrete. *Functl Mater* 46:84–87.
32. Ma Cong (017) Research on efficient curing agents and strength characteristics of cured soil in saturated soft soil. Shanghai Jiao tong University, 2017.

33. WANG Tian, WENG Xingzhong, ZHANG Jun, et al. (2017) Experimental study on compressive strength of composite cured sandy soil under dry and wet cycle conditions. *J Railway Sci Eng* 14: 721–729.
34. Yan Xiaowei (2020) Experimental study on the effect of freezing and thawing on the properties of river silt bubble mixed soil. Suzhou University of Science and Technology, 2020.
35. Zhou Cuiying, Zhao Shanshan, Yang Xu,et al. (2019) Application of ecological ester materials for sand soil improvement and engineering slope protection. *Geotechnics* 40: 4828–4837.
36. LI Guoxun, ZHANG Yanmei, MARTIN, et al. (2020) Effect of fiber on the mechanical properties of nanosilica lime-amended chalk. *J Civil Environ Eng* 42: 37–44.
37. ZHANG Jianwei, LU Zizhuang, LI Xiang, et al. (2025) Durability of polypropylene fibers on enzyme-induced carbonate precipitation-cured sandy soil under dry and wet cycling. *J Compos Mater* 42: 1000–1009. DOI:10.13801/j.cnki.fhclxb.20240521.006.
38. Liang Pentao (2018) Experimental research on mechanical properties and durability of air bubble lightweight soil. Hebei University of Architecture and Engineering, 2018.
39. Deng J (2023) Research on the effect of PVA fiber admixture on the performance of high-performance sprayed waterproof concrete. *China Build Waterproofing* 2023: 53–56. DOI: 10.15901/j.cnki.1007-497x.2023.02.012.
40. WANG Liming, LIU Shiguang, WANG Caixia, et al. (1997) Effect of specimen length on mechanical properties of fibers. *Text J* 1997: 7-8+3. DOI: 10.13475/j.fzxb.1997.04.002.
41. Niu Weiwei (2019) Research on the mechanical properties of basalt fiber-cement improved soil under freeze-thaw cycle. Beijing Jiaotong University, 2019.
42. Tian Jiayi (2019) Analysis of mechanical properties and reinforcement mechanism of fibrous soil under freeze-thaw action. Northeast Forestry University, 2019.
43. NING Xingtao, TAO Zhong, HUANG Ronggui, et al. (2024) Study on the improvement of properties of phosphorus building gypsum matrix composites by polyvinyl alcohol fibers. *Mater Her* 38: 646–650.
44. Wu J Q, Li B, Chen Y T, et al. (2023) Effects of polyethylene fiber content and length on the properties of high-tensile-strength engineered geopolymer composite. *J Mater Civ Eng* 35: 04023224. https://doi.org/10.1061/JMCEE7.MTENG-14763
45. Xie L, Sun X, Yu Z, et al. (2024) Effects of nano-silica on fracture properties and mechanism analysis of basalt fiber reinforced concrete. *Constr Build Mater* 439: 137375. https://doi.org/10.1016/j.conbuildmat.2024.137375
46. Fan Jinyuan, Jiang Yi, Wang Limin, et al. (2020) Study on sulfate erosion resistance of sisal-PVA hybrid fiber-reinforced geopolymer. *Silic Bull* 39:1430-1437+1443.
47. WANG Zhenshan, ZONG Mengyuan, ZHAO Kai,et al. (2020) Experimental study on corrosion resistance and mechanical properties of basalt fiber concrete under sodium sulfate environment. *Build Struct* 50: 118-123+37.
48. Zhang S, He S, Ghiassi B, et al. (2023) Interface bonding properties of polyvinyl alcohol (PVA) fiber in alkali-activated slag/fly ash. *Cem Concr Res* 173: 107308. https://doi.org/10.1016/j.cemconres.2023.107308

AIMS Press

© 2025 the Author(s), licensee AIMS Press. This is an open access article distributed under the terms of the Creative Commons Attribution License (http://creativecommons.org/licenses/by/4.0)